DOI: 10.61782/fa.2023.1024

forum acusticum 2023

OPTIMIZING THE POSITION OF SENSORS FOR CHARACTERIZING ACOUSTIC FIELDS

Samuel A. Verburg[1*] **Filip Elvander**[2] **Toon van Waterschoot**[3]
Efren Fernandez-Grande[1]
[1] Department of Electrical and Photonics Engineering, Technical University of Denmark, Denmark
[2] Department of Information and Communications Engineering, Aalto University, Finland
[3] Department of Electrical Engineering, ESAT-STADIUS, KU Leuven, Belgium

ABSTRACT

Characterizing acoustic fields over space is required in sound field analysis, spatial audio, as well as several applications within room acoustics and virtual reality. In order to measure a sound field over medium/large volumes, a large number of sensors have to be distributed over space. In this study we investigate optimal distributions of sensors for capturing acoustic fields in space. The positions are selected to maximize the sampled information and minimize the uncertainty in the reconstructed field. We show that the proposed optimization substantially reduces the amount of measurements in comparison to uniform or randomized distributions. The proposed optimal selection procedure can also be significant for other data-scarce applications.

Keywords: *sensor selection, sound field reconstruction, optimal sampling*

1. INTRODUCTION

The characterization of sound fields over space is central to acoustic research, e.g., in sound field control [1], spatial audio [2], source localization [3], and analysis of room acoustics [4]. One of the biggest challenges when characterizing sound fields over space is the large number of measurements required, which increases with frequency and size of the sampled domain [5]. Therefore, optimizing the distribution of measurement is very valuable, as it can extend the bandwidth and size of the reconstructed sound field for a given number of microphones, or alternatively, reduce the sampling requirements for a given reconstruction accuracy.

The design of microphone distributions over space has been partly guided by stability criteria. Spherical arrays, in which microphones are placed on the surface of a sphere, is one of the most popular microphone array configurations [6]. In general, it is beneficial to place most of the available sensors on the boundary of the sampled domain [7], regardless of its shape. However, placing all the sensors on the domain's boundary leads to instabilities at the domain's eigenfrequencies [6,8]. Such instabilities are a well-known problem of open array configurations, and several strategies exist to increase the robustness, including flush-mounting the microphones on a rigid sphere [9], using directional microphones [10], or placing a fraction of the sensors in the interior of the domain [7, 8, 11]. The optimization of interior positions to stabilize open arrays has been studied for spherical, cubic and ellipsoidal domains [8,11]. However, in applications such as sound field control and spatial audio, there might be restrictions as to where the sensors can be placed [12, 13], e.g., if the sensors can only be placed *around*, but not *inside*, the domain of interest.

In this extended abstract we examine the optimization of sensor positions for characterizing acoustic fields. We outline a selection method that aims at minimizing the error when estimating the amplitude of the waves that compose the sound field (presented in [14]), and we propose an extension in which the goal is to minimize the error when estimating the pressure in the reconstruction area. We present results for a test case and compare the perfor-

**Corresponding author*: *saveri@dtu.dk.*

mance of the proposed methods with a uniform sampling on the boundary and random sampling distributions.

2. METHOD

2.1 Model

A harmonic pressure field, $y(\mathbf{r})e^{j\omega t}$, at frequency ω and inside the domain Ω ($\mathbf{r} \in \Omega$, and $\Omega \subset \mathbb{R}^3$) can be described as a superposition of plane waves [15], such that

$$\mathbf{y} = \mathbf{A}\mathbf{x} + \mathbf{e}, \tag{1}$$

where $\mathbf{y} \in \mathbb{C}^M$ is the vector of pressure values at positions $\mathbf{r}_1, \ldots, \mathbf{r}_M$. The matrix $\mathbf{A} \in \mathbb{C}^{M\times N}$, with elements $a_{ij} = e^{j\mathbf{k}_j \cdot \mathbf{r}_i}$, represents the plane wave expansion. Here, $\mathbf{k}_j \in \mathbb{R}^3$ is the wavenumber vector of the j^{th} plane wave. The wavenumber components are uniformly sampled on the surface of the radiation sphere with radius ω/c, where c is the speed of sound. [1] The vector $\mathbf{x} \in \mathbb{C}^N$ contains the amplitude and phase of the N plane waves, which are to be estimated from the measurements. The vector $\mathbf{e} \in \mathbb{C}^M$ accounts for additive measurement noise.

Once an estimation of the wave coefficient, $\tilde{\mathbf{x}}$, is obtained, the pressure at any set of positions $\mathbf{s}_1, \ldots \mathbf{s}_L \in \Omega$ can be reconstructed via

$$\mathbf{y}_B = \mathbf{B}\tilde{\mathbf{x}}, \tag{2}$$

where $\mathbf{y}_B$ is the pressure at the reconstruction positions, and $\mathbf{B} \in \mathbb{C}^{L\times N}$, with elements $b_{ij} = e^{j\mathbf{k}_j \cdot \mathbf{s}_i}$, is the reconstruction matrix.

Optimal sensor placement aims at selecting the S sensor positions from the M candidates that are optimal to estimate the sound field. The selection is represented by the activation vector $\mathbf{z} = [z_1, ..., z_M]^T$, with $z_i \in \{0, 1\}$ indicating whether the i^{th} sensor is selected or not. The selection matrix, $\mathbf{Z} \in \{0, 1\}^{S\times M}$, results from removing the zero-rows from $\text{Diag}(\mathbf{z})$. It is noted that $\mathbf{Z}^T\mathbf{Z} = \text{Diag}(\mathbf{z})$. The selected pressure measurements, $\mathbf{y}_z$, are obtained by multiplying both sides of Eq. (1) with the selection matrix,

$$\mathbf{y}_z = \mathbf{Z}\mathbf{y} = \mathbf{Z}\mathbf{A}\mathbf{x} + \mathbf{Z}\mathbf{e}. \tag{3}$$

2.2 Estimation

The estimation of $\mathbf{x}$ is addressed in the Bayesian framework. The measurement noise is modeled as i.i.d. Gaussian with variance β^{-1}. The likelihood is then

$$p(\mathbf{y}_z|\mathbf{x}, \beta) = \mathcal{CN}(\mathbf{y}_z|\mathbf{A}\mathbf{x}, \beta^{-1}\mathbf{I}). \tag{4}$$

We assign a Gaussian prior distribution with variance α^{-1} to the wave coefficients, such that

$$p(\mathbf{x}|\alpha) = \mathcal{CN}(\mathbf{x}|\mathbf{0}, \alpha^{-1}\mathbf{I}). \tag{5}$$

The posterior distribution is found via Bayes' theorem,

$$p(\mathbf{x}|\mathbf{y}_z, \alpha, \beta) \propto p(\mathbf{y}_z|\mathbf{x}, \beta)p(\mathbf{x}|\alpha) = \mathcal{CN}(\mathbf{x}|\tilde{\mathbf{x}}, \boldsymbol{\Sigma}), \tag{6}$$

where $\tilde{\mathbf{x}}$ is the maximum a posteriori estimate,

$$\tilde{\mathbf{x}} = \beta\boldsymbol{\Sigma}\mathbf{A}^{\text{H}}\mathbf{Z}^{\text{H}}\mathbf{y}_z, \tag{7}$$

and $\boldsymbol{\Sigma}$ is the covariance matrix,

$$\boldsymbol{\Sigma} = (\beta\mathbf{A}^{\text{H}}\mathbf{Z}^{\text{H}}\mathbf{Z}\mathbf{A} + \alpha\mathbf{I})^{-1}. \tag{8}$$

The estimate $\tilde{\mathbf{x}}$ corresponds to the least squares ℓ_2-norm regularized solution [16], and it is determined by the covariance matrix $\boldsymbol{\Sigma}$, which in turn depends on the selected sensors via $\mathbf{Z}$.

2.3 Optimization problem

The mean squared error of any estimator is lower bounded by the Bayesian Cramér-Rao bound [17],

$$\mathbb{E}\left\{(\tilde{\mathbf{x}} - \mathbf{x})(\tilde{\mathbf{x}} - \mathbf{x})^{\text{H}}\right\} \succeq \mathbf{F}^{-1} \tag{9}$$

where $\mathbf{F}$ is the Bayesian Fisher information matrix, defined as

$$\mathbf{F} \triangleq \mathbb{E}\left\{\nabla_{\mathbf{x}^*} \log p(\mathbf{y}, \mathbf{x}) \left[\nabla_{\mathbf{x}^*} \log p(\mathbf{y}, \mathbf{x})\right]^{\text{H}}\right\}, \tag{10}$$

implying that

$$\mathbb{E}\left\{|x_i - \tilde{x}_i|^2\right\} \geq \mathbf{F}^{-1}_{ii}, \tag{11}$$

i.e., the mean squared error when estimating the i^{th} wave coefficient is lower bounded by the i^{th} element of the diagonal of $\mathbf{F}^{-1}$. For the model described in Sections 2.1 and 2.2 it can be shown that $\boldsymbol{\Sigma} = \mathbf{F}^{-1}$.

We formulate the optimal selection as the problem of finding the sensors that minimize the mean squared error when estimating the wave coefficients [14]. The optimization problem is then

$$\mathbf{z} = \arg\min \text{ tr}(\boldsymbol{\Sigma}) \quad \text{s.t.} \quad ||\mathbf{z}||_0 = S\,,\, z_i \in \{0, 1\}\,, \tag{12}$$

[1] This representation is valid assuming that Ω is convex, no sound sources are inside Ω, and Ω is relatively far from any source so that the evanescent field can be ignored.

where $\mathrm{tr}(\mathbf{\Sigma})$ denotes the trace of $\mathbf{\Sigma}$. The optimization problem (12) is S-choose-M combinatorial, and finding an exact solution by sweeping through all possible combinations is intractable. [18, 19] In this study we approximate the solution to (12) via convex relaxation [19–21].

The selection problem (12) yields a sensor distribution that is optimal in terms of estimating $\mathbf{x}$. However, it is often required to accurately recover the pressure in a given domain, but not the wave coefficients. We therefore propose an extension of the method, in which the sensors that minimize the mean squared error of the reconstructed pressure, $\mathbf{Bx}$, are selected. In this case the optimization problem becomes,

$$\mathbf{z} = \arg\min\ \mathrm{tr}(\mathbf{B\Sigma B}^{\mathrm{H}}) \quad \text{s.t.} \quad ||\mathbf{z}||_0 = S\,,\, z_i \in \{0,1\}\,. \tag{13}$$

The reason for choosing to minimize the error in estimating $\mathbf{Bx}$ is that a large error in estimating $\mathbf{x}$ does not necessarily translates into a large error in estimating $\mathbf{Bx}$. In addition, applications such as sound field control and virtual sensing require to predict the pressure at a region where sensors cannot be placed (e.g., inside a listening or control area), regardless of the coefficients used to describe the sound field.

Both optimization methods can be extended to account for several frequencies simultaneously by minimizing a sum of covariance matrices, so that problem (12) becomes

$$\mathbf{z} = \arg\min \sum_{j=1} \mathrm{tr}(\mathbf{\Sigma}_j) \quad \text{s.t.} \quad ||\mathbf{z}||_0 = S\,,\, z_i \in \{0,1\}\,, \tag{14}$$

where $\mathbf{\Sigma}_j$ is the covariance matrix for the j^{th} frequency used in the optimization [defined in Eq. (8)]. Problem (13) can be modified in the same way.

3. RESULTS

A numerical experiment is conducted for the configuration shown in Fig. 1. The reconstruction area is defined as an ellipse with principal axes of length 1 m and 0.4 m (yellow area in Fig. 1). The measurement area is defined as the difference between the reconstruction area and a rectangle of sides 1.4 m and 0.7 m (red area in Fig. 1). Both areas are discretized into small elements of approximately 3 cm using a uniform triangular mesh [22]. The number of candidate positions M is 866, the sensor budget S is set to 78, and the number of positions inside the reconstruction area L is 395. The experiment is performed in 2D for the sake of clarity. The extension to the 3D case is straight forward.

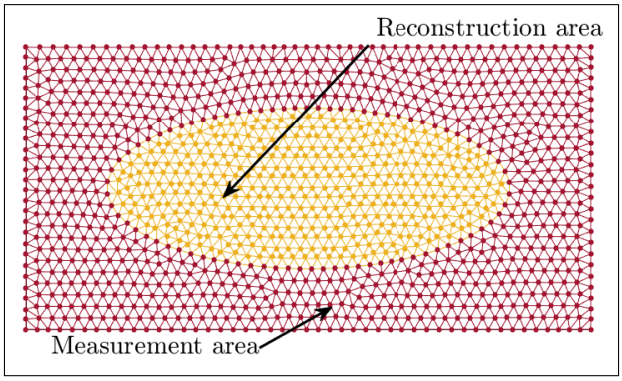

Figure 1. Setup of the numerical study.

Figure 2 shows the sensor distributions examined in this study. Figure 2(a) corresponds to the uniform sampling of the boundary enclosing the reconstruction domain. Figure 2(b) corresponds to a random selection of samples from the candidate positions. Figure 2(c) corresponds to the sensor selection optimized to estimate $\mathbf{x}$, and Fig. 2(d) to the selection optimized for reconstructing $\mathbf{Bx}$, as described in Section 2.3. The frequency used for the optimization in both cases is 1 kHz. The multi-frequency selection of problem (14) was also tested, using the ellipse eigenfrequencies in the optimization. The resulting distributions were rather similar to the ones obtained using only 1 kHz, with slightly lower errors when the single frequency was used. The results shown henceforth are for the optimization with 1 kHz. The selection optimized for estimating the wave coefficients [Fig. 2(c)] places a large fraction of the available sensors on the outer boundary of the measurement area (along the sides of the rectangle). On the contrary, the selection optimized for estimating the pressure inside the reconstruction area [Fig. 2(d)] concentrates many samples on the boundary of the ellipse. We observe that none of the optimized selections places *all* of the sensors on the boundaries of the measurement domain.

A quantitative comparison across frequency is shown in Fig. 3. Figure 3(a) shows the condition number of $\mathbf{ZA}$, defined as the ratio between its maximal and minimal singular values. The condition number is a measure for the robustness of the estimation of $\mathbf{x}$ to errors in the measurements, and it has been used as a criterion for the design of microphone arrays [11]. A large condition number in-

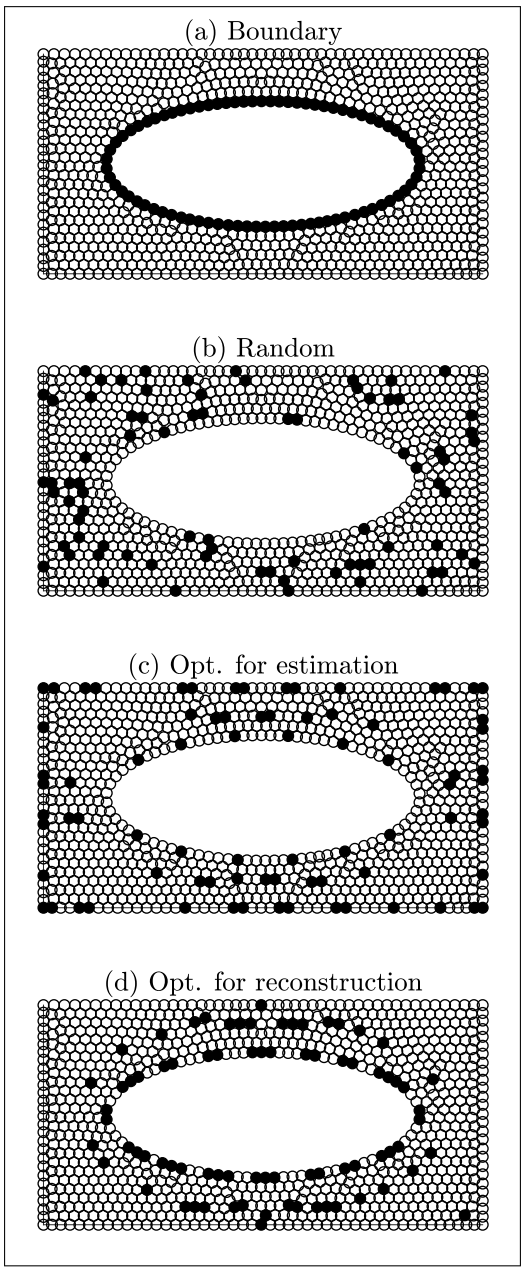

Figure 2. Sensor distributions. White circles indicate the non-selected candidate positions, black circles indicate the selected positions. (a) Uniform sampling on the boundary of the reconstruction area. (b) Random selection of samples. (c) Selection optimized for the estimation of $\mathbf{x}$. (d) Selection optimized for the reconstruction $\mathbf{Bx}$. All distributions comprise of the same number of sensors, $S = 78$.

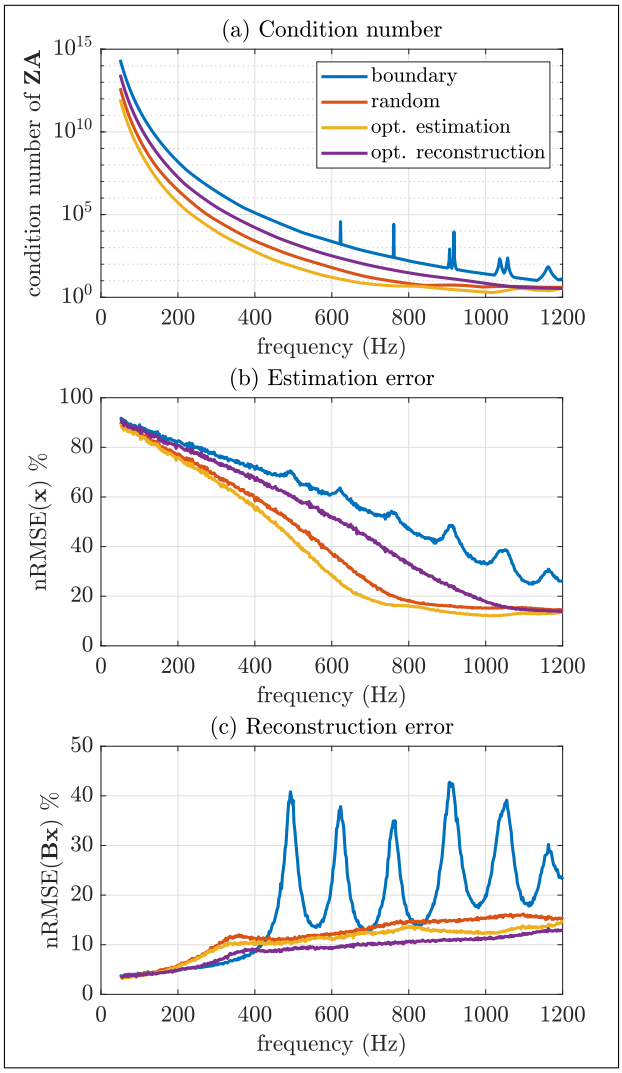

Figure 3. Results for the sensor distributions of Fig. 2 over frequency. (a) Condition number of $\mathbf{ZA}$. (b) Error in the estimation of $\mathbf{x}$. (c) Error in the reconstruction $\mathbf{Bx}$.

dicates that small changes in the input, such as noise, get largely amplified in the estimation. Figure 3(a) shows that the boundary sampling is unstable at the eigenfrequencies of the elliptical reconstruction area (large condition numbers at frequencies 622 Hz, 761 Hz, 906 Hz, etc.). The other three distributions (random and optimized) avoid the instability at such frequencies by distributing sensors over the whole candidate area. Placing a large fraction of the available sensors on the outer boundary, far from the center, seems to reduce the condition number. This can be seen particularly for the selection optimized for estimating $\mathbf{x}$, [Fig. 2(c)] as it is the distribution that achieves the smallest condition number of them all [yellow curve in Fig. 3(a)].

The estimation and reconstruction errors are examined by means of a Monte Carlo simulation. We generate $K = 500$ instances of a random vector of coefficients $\mathbf{x}$ by drawing independent samples from a normal distribution. Noisy measurements are then computed for each of the sensor distributions of Fig. 2. The variance of the noise and coefficients, β^{-1} and α^{-1}, are chosen to yield a SNR of approximately 13 dB. The MAP estimate $\tilde{\mathbf{x}}$ for each sound field is computed via Eq. (7). The pressure field in the reconstruction area is computed via Eq. (2), where $\mathbf{B}$ is the reconstruction matrix for the positions inside the ellipse.

The normalized root mean squared error (nRMSE) for the estimation of $\mathbf{x}$ is calculated as

$$\text{nRMSE}(\tilde{\mathbf{x}}) = \sqrt{\frac{\sum_{i=1}^{K} \text{tr}\left[(\tilde{\mathbf{x}}_i - \mathbf{x}_i)(\tilde{\mathbf{x}}_i - \mathbf{x}_i)^{\text{H}}\right]}{\sum_{i=1}^{K} ||\mathbf{x}_i||_2^2}}. \quad (15)$$

The nRMSE for the reconstruction is calculated by replacing $\mathbf{x}_i$ and $\tilde{\mathbf{x}}_i$ for $\mathbf{B}\mathbf{x}_i$ and $\mathbf{B}\tilde{\mathbf{x}}_i$, respectively, in Eq. (15).

Figure 3(b) shows the normalized error when estimating $\mathbf{x}$ for the different distributions. A general trend of larger estimation errors at lower frequencies is observed, in agreement with the condition number results [Fig. 3(a)]. The uniform distribution on the ellipse boundary presents the largest error of all the studied distributions. In particular, the instabilities at the eigenfrequencies lead to a high error at such frequencies [peaks in blue line of Fig. 3(b)]. The selection optimized for reconstructing the pressure field [purple line in Fig. 3(b)] avoids the instabilities at the eigenfrequencies, despite placing a large fraction of sensors on the boundary of the ellipse [Fig. 2(d)]. The lowest estimation error is achieved by the selection optimized for estimating $\mathbf{x}$ [yellow line in Fig. 3(b)], demonstrating the effectiveness of the optimization method.

Figure 3(c) shows the normalized error when reconstructing $\mathbf{B}\mathbf{x}$ for the different distributions. In general, the reconstruction error increases with frequency. At low frequencies the simulated sound fields are rather even over the reconstruction area, [2] and thus the exact recovery of $\mathbf{x}$ is not critical for a successful estimation of $\mathbf{B}\mathbf{x}$ – as long as the overall level is correctly recovered. The selection optimized for reconstructing the pressure field achieves the lowest error over the entire frequency range [purple line in Fig. 3(c)], with approximately 5% improvement with respect to the random sampling and the other optimized distribution [red and yellow lines in Fig. 3(c)]. The boundary sampling [blue line in Fig. 3(c)] presents very large reconstruction errors at the eigenfrequencies. The results indicate that the condition number of $\mathbf{ZA}$ or the estimation error might not be the best guiding criteria for the selection of microphone positions in applications where the goal is to reconstruct a sound field over space (e.g., sound filed control and spatial audio). The results show more accurate reconstructions of the pressure field when the covariance matrix of $\mathbf{B}\mathbf{x}$ is used in the optimization. Therefore, the choice objective function in the optimal sensor placement depends on the application, e.g., in source localization it is interesting to estimate the wave amplitudes $\mathbf{x}$ [solution to problem (12)], while in sound field control and virtual sensing it is of interest to recover the pressure in the reconstruction area $\mathbf{B}\mathbf{x}$ [solution to problem (13)].

4. CONCLUSION

The optimal selection of sensor positions for characterizing acoustic fields have been investigated, and two selection methods have been examined. In the first method the objective is to find the sensors that lead to the minimum mean squared error in the estimation of the wave coefficients that describe the sound field. In the second method the goal is to find the sensor positions that result in the minimum mean squared error in the estimation of the pressure over the reconstruction area. A numerical study shows that the optimized distributions outperform a uniform distribution on the boundary of the reconstruction area and a random distribution over the measurement

[2] This is due to (a) at low frequencies (lower than approximately 350 Hz) the wavelengths are larger than the reconstruction area, and (b) in the Monte Carlo simulation the wave coefficients are independent and identically distributed.

area. The results demonstrate that the optimized distributions archive lower errors over a large frequency range, despite them being optimized for a single frequency. We anticipate that the proposed optimal selection methods can be relevant for other data-scarce applications.

5. ACKNOWLEDGMENTS

The work was supported by a research grant from the VILLUM foundation (grant no. 19179, "Large-scale acoustic holography").

6. REFERENCES

[1] T. Betlehem, W. Zhang, M. A. Poletti, and T. D. Abhayapala, "Personal sound zones," *IEEE Signal Process. Mag.*, vol. 32, no. 2, pp. 81–91, 2015.

[2] W. Zhang, P. N. Samarasinghe, H. Chen, and T. D. Abhayapala, "Surround by sound: a review of spatial audio recording and reproduction," *Appl. Sci.*, vol. 7, no. 5, 2017.

[3] M. Hahmann, E. Fernandez-Grande, H. Gunawan, and P. Gerstoft, "Sound source localization using multiple ad hoc distributed microphone arrays," *JASA Express Lett.*, vol. 2, no. 7, 2022.

[4] M. Nolan, "Estimation of angle-dependent absorption coefficients from spatially distributed in situ measurements," *J. Acoust. Soc. Am.*, vol. 147, no. 2, pp. EL119–EL124, 2020.

[5] T. Ajdler, L. Sbaiz, and M. Vetterli, "The plenacoustic function and its sampling," *IEEE Trans. Sig. Proc.*, vol. 54, no. 10, pp. 3790–3804, 2006.

[6] B. Rafaely, "Analysis and design of spherical microphone arrays," *IEEE Trans. Audio, Speech, Lang. Process.*, vol. 13, no. 1, pp. 135–143, 2005.

[7] G. Chardon, A. Cohen, and L. Daudet, "Sampling and reconstruction of solutions to the Helmholtz equation," *Sampl. Theory Signal Image Process.*, vol. 13, no. 1, pp. 67–89, 2014.

[8] G. Chardon, W. Kreuzer, and M. Noisternig, "Design of spatial microphone arrays for sound field interpolation," *IEEE J. Sel. Topics Signal Process.*, vol. 9, no. 5, pp. 780–790, 2015.

[9] J. Meyer and E. Gary, "A highly scalable spherical microphone array based on an orthonormal decomposition of the soundfield," in *Proc. of the IEEE International Conference on Acoustics, Speech, and Signal Processing, ICASSP 2002*, (Orlando, FL, USA), 2002.

[10] I. Balmages and B. Rafaely., "Open-sphere designs for spherical microphone arrays," *IEEE Trans. Audio, Speech, Lang. Process.*, vol. 15, no. 2, pp. 727–732, 2007.

[11] B. Rafaely, "The spherical-shell microphone array," *IEEE Trans. Audio, Speech, Lang. Process.*, vol. 16, no. 4, pp. 740–747, 2008.

[12] S. Koyama, G. Chardon, and L. Daudet, "Optimizing source and sensor placement for sound field control: an overview," *IEEE/ACM Trans. Audio, Speech, Language Process.*, vol. 28, pp. 696–714, 2020.

[13] T. Nishida, N. Ueno, S. Koyama, and H. Saruwatari, "Sensor placement in arbitrarily restricted region for field estimation based on gaussian process," in *Proc. of the 28th European Signal Processing Conference, EUSIPCO 2021.*, (Dublin, Ireland), 2021.

[14] S. A. Verburg, F. Elvander, T. van Waterschoot, and E. Fernandez-Grande, "Optimal sensor placement for sound field reconstruction," in *Proc. of the 24rd International Congress on Acoustics, ICA 2022.*, (Gyeongju, Korea), 2022.

[15] E. G. Williams, *Fourier acoustics - sound radiation and nearfield acoustic holography*. San Diego: Academic Press, 1999.

[16] J. M. Bardsley, *Computational uncertainty quantification for inverse problems*. Philadelphia, PA, USA: SIAM, 2018.

[17] H. L. V. Trees and K. L. Bell, *Bayesian bounds for parameter estimation and nonlinear filtering/tracking*. New York, NY, USA: Wiley-IEEE press, 2007.

[18] A. Krause, A. Singh, and C. Guestrin, "Near-optimal sensor placements in Gaussian processes: theory, efficient algorithms and empirical studies.," *J. Mach. Learn. Res.*, vol. 9, no. 2, pp. 235–284, 2008.

[19] S. Joshi and S. Boyd, "Sensor selection via convex optimization," *IEEE Trans. Signal Process.*, vol. 57, no. 2, pp. 451–462, 2009.

[20] S. P. Chepuri and G. Leus, "Sparsity-promoting sensor selection for non-linear measurement models," *IEEE Trans. Signal Process.*, vol. 63, no. 3, pp. 684–698, 2015.

[21] J. Swärd, F. Elvander, and A. Jakobsson, "Designing sampling schemes for multi-dimensional data," *Signal Process.*, vol. 150, pp. 1–10, 2018.

[22] P.-O. Persson and G. Strang, "A simple mesh generator in MATLAB," *SIAM Review*, vol. 46, no. 2, pp. 329–345, 2004.